Nitric oxide detection using catalytic properties of CuCo-PTC metal-organic framework

Meng Wang
Hui Dong (huidong607607@126.com)
Zhengzhou University
Yintang Zhang
Yanli Zhou
Mengjiao Gu
Qianqian Zhu
Yiwen Song
Baoxian Ye
Maotian Xu

Short Report

Keywords: CuCo-PTC MOF materials, Nitric oxide, Gas sensor, Highly sensitive detection

Posted Date: February 28th, 2022

DOI: https://doi.org/10.21203/rs.3.rs-1110735/v1

Abstract

Nitric oxide is one of the atmospheric pollutants and an important gas messenger molecule in the human body, involved in many physiological and pathological processes. Therefore, detecting nitric oxide rapidly and accurately has been one of the popular topics in recent decades. In this study, we synthesized CuCo-PTC MOF materials using a solvothermal method based on the mechanism of triazole ring formation from o-phenylenediamine (OPD) and nitric oxide. The synthesized CuCo-PTC MOF materials show high sensitivity and good selectivity for detecting nitric oxide in vitro and in cell lysates. The results indicate the potential for applying this sensing strategy to detect nitric oxide in the internal environment.

1. Introduction

Nitric Oxide (NO), one of the intracellular molecules, plays an important role in the immune system and in the vasodilator pathway of the human nervous system [1]. However, excessive NO can lead to many pathological reactions, such as atherosclerosis, diabetes, angiogenesis, Parkinson's disease, and Alzheimer's disease [2–4]. It is difficult to determine the sub-micromolar concentration of NO under certain physiological pH conditions because it is a short-lived, rapidly diffusing gas molecule. NO is present in both vehicle exhaust and thermal power plant exhaust, and therefore, plays an important role in environmental science. Additionally, the increase of NO in the atmosphere may cause harmful phenomena, such as acid rain and smog [5–7]. Therefore, the quantitative detection of NO is important both in biomedicine and in pollution monitoring.

At present, standard NO detection techniques include UV-Vis, chemiluminescence, electrochemistry, and mass spectrometry [8–12]. The majority of these testing methods require complex sample pre-treatment, specialised technicians, and expensive testing costs, limiting the application of NO detection. For example, Ridnour et al. [8] demonstrated a spectrophotometric method for the determination of NO in tissue culture media. The detection strategy uses a nitrosative modification of sulphoraphane mediated by NO, which reacts with N-(1-naphthyl) ethylenediamine dihydrochloride to produce an orange product with strong UV-vis absorption at 496 nm. The method is easy to apply but not sensitive enough to detect NO. Wu et al. [9] developed two electrochemiluminescence sensors based on a metal-organic framework (MOF) for NO, Cu-TCA, and Eu-TCA detection by introducing the triphenylamine fraction as a bright blue emitter. Although they achieved good detection sensitivity, the method was complex and demanding for non-specialists. Goodwin et al. [10] described a way to directly measure NO in aqueous solutions using membrane inlet mass spectrometry (MIMS). The method achieved good sensitivity and linear detection range, better than most detection methods for NO, but the detection cost was too high for practical applications of NO detection. Optical sensing strategies are considered the most convenient and rapid means of detection owing to their intuitive visual variation, high sensitivity, and relatively low detection costs, with fluorescence spectroscopy favoured as the most sensitive. This was the motivation behind our interest in devising a fluorescence and colourimetry-based method for NO detection.

O-Phenylenediamine (OPD) is a cheap, non-absorbing, non-fluorescent organic molecule, which can be oxidized to 2,3-diaminophenothiazine (OPDox) by metal ions (Cu^{2+} and Fe^{2+}) and H_2O_2 [14]. OPDox can serve as an indicator for organic molecules in spectroscopic detection techniques because of its absorption and fluorescent signal. However, the oxidation of OPD by metal ions or H_2O_2 is slow, and therefore, does not allow for easy and fast detection of NO [15]. Li's group [13] proposed a solution using metal ions and hydrogen peroxide to co-oxidize OPD, thus increasing the reaction rate. In addition, reducing the activation energy of chemical reactions can also increase the reaction rate. For example, Chen et al. [15] used Cu^{2+} catalysis to accelerate OPD oxidation by hydrogen peroxide. Although the detection achieved good sensitivity, the reaction was slow, and the reaction temperatures needed to stay high. It was, therefore, necessary to speed up the reaction rate at room temperature. MOFs, also known as biocatalysts for reactions, could inspire new ideas for applying this excellent small indicator molecule (OPD).

MOFs have already become an exciting material with an excellent porous structure with attractive properties, such as regular channels, high specific surface area, moderate functionalisation capabilities, structural diversity, and abundant metal sites [16–20]. These unique properties give MOF materials excellent performance in the fields of energy gas storage, adsorption and separation of gases and liquids, separation of membrane materials, biomedicine, optoelectronics, magnetic sensing, etc. [16–25]. Its application to non-homogeneous catalysis is also a major research focus [19, 26]. Li et al. [26] showed that MIL-88B MOF materials have good selective catalytic properties.

In this work, we synthesized CuCo-PTC MOF materials using the solvothermal method. The CuCo-PTC MOF materials were then used as chemical reaction catalysts to detect NO using fluorescence and colourimetry, they exhibited perfect catalytic properties when used in the reaction of hydrogen peroxide oxidizing OPD, which significantly increased the reaction rates. In the oxidation reactions of OPD, NO reacts first with OPD to form N-(2-hydrazinophenyl) methylamine when added to NO. However, N-(2-hydrazinophenyl) methylamine will not be oxidized by hydrogen peroxide to produce OPDox with fluorescence emission, which results in NO detection (Fig.1). This sensing strategy for NO has a short detection time and offers excellent sensitivity and selectivity.

2. Materials And Methods

2.1 Materials

All initial raw materials were purchased from commercial sources and could be used without further purification. Anhydrous ethanol and N, N-dimethylformamide (DMF) were obtained from Tianjin Jindong Tianzheng Fine Chemical Reagent Factory (Tianjin, China). In addition, methanol (99.5%), copper nitrate (99.5%), disodium hydrogen phosphate (99.0%), sodium dihydrogen phosphate (99.0%) and cobalt chloride (99.5%) were purchased from Tianjin Beichen Foundry Reagent Factory (Tianjin, China). Biphenyl-(3,4',5)-tricarboxylic acid (99.5%) was purchased from Shanghai Tengqian Biotechnology Co. S-nitroso-N-acetyl penicillamine (SNAP) was purchased from Sigma Aldrich Trading Co. Cell lysate solution

was purchased from Beijing Dingguo Changsheng Biotechnology Co. Ultra-pure water (18.2 MΩ·cm^{-1}) was purified using a Mill-Q water purification system (Millipore, Bedford, France) throughout the study.

2.2 Instruments and equipment

Fluorescence emission spectra were recorded with a Perkin Elmer fluorescence spectrophotometer (Waltham, Massachusetts, USA). The appearance of CuCo-MOF was characterised by the Zeiss MERLIN Compact scanning electron microscope. The size and morphology of CuCo-PTC MOF were studied on a JEOL JEM 2100 transmission electron microscope. X-ray photoelectron spectroscopy was performed with a Thermo Scientific K-Alpha X-ray diffraction spectroscope. The structural changes were observed with a Bruker D8 Advance X-Ray powder diffractometer. The infrared spectra were recorded on a Thermo Scientific Nicolet iS10 Fourier infrared spectroscope. Thermogravimetric analysis was performed on a TG 209F1 thermogravimetric analyser. The physical adsorption and desorption of nitrogen were studied with a MacTriStar II 3FlexTriStar II 3Flex specific surface and porosity analyser.

2.3 Synthesis of CuCo-PTC MOF

Biphenyl-(3,4',5)-tricarboxylic acid was first dissolved in a solvent mixture of 20 mL DMF and 2 mL ethanol at 50 °C with stirring until completely dissolved. Subsequently, 10 mmol·L^{-1} of $Cu(NO_3)_2{\cdot}6H_2O$ and 10 mmol·L^{-1} of $CoCl_2{\cdot}6H_2O$ were added to the mixture and stirred until completely dissolved. The dissolved solution was quickly transferred to the 45 mL polytetrafluoroethylene autoclave, heated at 170 ℃ for 16 h, cooled to room temperature, and centrifugated to obtain precipitation after the end of the reaction. The obtained MOF was washed with DMF, ethanol, and methanol three times. Finally, the washed MOF was placed in a vacuum drying oven at 35 ℃ for 12 h and dried to obtain the purple powder CuCo-PTC MOF.

2.4 Preparation of standard NO solution

We performed laboratory testing by using the simplified reporting method to prepare the NO testing solution. SNAP is organic matter that can release NO in an aqueous solution and quantitatively release NO at 1×10^{-12} mol·L^{-1} to 1×10^{-3} mol·L^{-1} in solution. We used SNAP and phosphate buffer solution (PBS) solution to prepare the standard NO solution.

2.5 NO sensing measurements

We prepared 450 μL of 0.1 mol·L^{-1} PBS (pH = 7.4), 12 μL of 0.2 μmol·L^{-1} OPD, and different concentrations of NO, added them to 1 mL centrifugal tubes, and incubated for 2 min. Subsequently, we added 12 μL of 0.2 μmol·L^{-1} CuCo-PTC MOF and 12 μL 0.2 of μmol·L^{-1} hydrogen peroxide to the above solution. We collected the relevant data at an incident wavelength of 520 nm on a fluorescence spectrometer after reacting for 6 min.

2.6 Spiked recovery of cell lysates

We evaluated the potential of the system to detect NO in actual samples using the recovery rate after adding NO in cell lysates with fluorescence colourimetric methods. We detected the NO concentrations in different samples by adding 5 μmol·L^{-1} SNAP standard solution with different volumes to the same volumes of cell lysates. Subsequently, we validated the applied potential of the sensing methods by using fluorescence colourimetric methods to evaluate the recovery rate of NO with different concentrations in cell lysates.

3. Results And Discussion

3.1 Characterisation of CuCo-PTC MOF

CuCo-PTC MOF was prepared by the coordination polymerisation between Co, Cu, and H_3PTC in DMF and ethanol. The shape and dimension of the product were obtained by scanning electron microscopy (SEM) and transmission electron microscopy (TEM). Fig. 2a and 2b show the prepared CuCo-PTC MOF, which presents a rough surface, and stratified and disordered accumulation. The chemical composition was determined by energy dispersive X-ray spectroscopy (EDS), which showed that the CuCo-PTC MOF contains Cu, Co, O, and C elements, and that these elements have a uniform distribution in samples (Fig. 3). We also tested for organic ligands H_3PTC and CuCo-PTC MOF using Fourier transform infrared spectroscopy, as shown in Fig. S1a. The most important functional group of H_3PTC is carbonyl at 1700 cm^{-1}, which produces a red shift in the crystallisation process. The disappearance of the signal at 1700 cm^{-1} in CuCo-PTC MOF indicates that the carboxyl group of the organic ligand is fully protonated and bound to the organometallic ion and that the carbonyl absorption peak of CuCo-PTC MOF shifted to 1568 cm^{-1}. The X-ray diffraction testing for the organic ligand H_3PTC and CuCo-PTC MOF material showed that the removal of reaction solvent influences the changes in pore structure, which finally leads to the amorphisation of MOF. Therefore CuCo-PTC MOF material does not show a well-defined diffraction peak in its XRD pattern (Fig. S1b), like the organic ligand.

We also investigated the surface element composition and chemical state of CuCo-PTC MOF material. The X-ray photoelectron spectroscopy (XPS) measurement showed that Co atoms are in a metallic state corresponding to the Co^{2+} reduction, with the binding energy of 778.68 eV for Co $2p^{1/2}$. The increase in the binding energy of Co $2p^{1/2}$ in CuCo-PTC MOF compared to standard cobalt metal (BE = 778.2 eV) is due to N–ligand interaction (Fig. 4a) [13]. The nitrogen adsorption experiments to determine the structure of the holes of CuCo-PTC MOF, shown in Fig. 4b, revealed that CuCo-PTC MOF had a specific surface area of 16.5125g·cm^3. Finally, we conducted thermogravimetric analysis (TG) in the air at a slope of 10 ℃·min^{-1} to test the thermal stability of CuCo-PTC MOF. The curves showed three important weightlessness steps. As shown in Fig. 4c, the TG curve indicated that the thermal stability temperature was 450 ℃ owing to the decomposition of the tricarboxylate linker. The decomposition of the skeleton and the formation of mixed-valence Co_3O_4 happened at 0–90 ℃. Thermogravimetric analysis of CuCo-PTC MOF showed that it had high thermal stability at a specific temperature.

3.2 Design and detection mechanism of colourimetric probes

The use of colourimetric probes to detect NO (Fig. 2) showed that, when NO is not present, all OPD in the solution oxidizes to OPDox, and the hydroxyl radical is produced by CuCo-PTC MOF catalysis of H_2O_2. The fluorescence emission by hydroxyl radical changes the colour of the solution from colourless to yellow. When NO exists, the OPD in solution first reacts with NO to form N-(2-hydrazinophenyl) methylamine. When CuCo-PTC MOF and H_2O_2 were added to the reaction solution, the concentration of oxidizable OPD decreases with increasing NO concentration. Therefore, this sensing strategy is feasible for NO detection in terms of method design.

3.3 Feasibility of NO sensing

Fluorescence emission spectroscopy was performed on the solution containing 0.1 $mol·L^{-1}$ of PBS, 10 $mg·L^{-1}$ of CuCo-PTC MOF, 26 $\mu mol·L^{-1}$ of OPD and 12 $mol·L^{-1}$ of hydrogen peroxide. As Fig. 5 shows, when NO (6 $\mu mol·L^{-1}$) was added to the detection system, the fluorescence quenched at 568 nm at the excitation wavelength of 520 nm. These results show that fluorescence colourimetry can be used for NO detection.

3.4 Composition optimisation

The key to obtaining a good signification signal is the optimum composition of the reaction solution because the detection of NO by fluorescence colourimetry involves the oxidation of OPD by hydrogen peroxide and related chemical reactions. First, we optimize the concentration of the PBS. As Fig. S2 shows, we investigated the concentration range of PBS between 0.001 $mol·L^{-1}$ and 0.1 $mol·L^{-1}$ in the NO detection system. For the PBS concentration of 0.1 $mol·L^{-1}$, the Uv-vis absorption of the gold nanoparticles solution reached the maximum, meaning that the optimum concentration of PBS is 0.1 $mol·L^{-1}$.

Next, we researched the influence of the concentration of the catalyzer CuCo-PTC MOF on the intensity of fluorescence signal in the detection system. As shown in Fig. S3, the fluorescence emission of the detection system reaches the maximum when the concentration of the CuCo-PTC MOF is 8 $mg·L^{-1}$.

We subsequently optimized the concentration of OPD, which acts as the fluorescent emitter in the detection system, as shown in Fig. S4. The fluorescence emission of the detection system reached the maximum when the concentration of OPD was 24 $\mu mol·L^{-1}$. We then optimized the concentration of H_2O_2, as shown in Fig. S5, the best concentration of H_2O_2 was 16 $mol·L^{-1}$. Finally, we also found that in the presence of CuCo-PTC MOF catalyst, the detection system could be oxidized by H_2O_2 within 5 min (Fig. S6).

3.5 Sensitivity

The fluorescent emission intensity of OPDox can be controlled by changing reaction conditions. The fluorescence intensity is proportional to the concentration of OPDox, and with the oxidation of OPD, the fluorescence intensity increases. The variation in composition can be directly measured because the signal change can be quantified. NO and OPD react to form N-(2-hydrazinophenyl) methylamine, which can indirectly change the concentration of OPDox. Therefore, it can achieve the purpose of detecting NO (Technological process 1). Under the optimum reaction conditions, the concentrations of the components were 0.1 mol·L^{-1} of PBS, 10 mg·L^{-1} of CuCo-PTC MOF, 26 μmol·L^{-1} of OPD, and 12 mol·L^{-1} of hydrogen peroxide. The fluorescence titration curve showed that with the increase in NO concentration, the fluorescence intensity at 568 nm decreased linearly (Fig. 6) until the concentration of NO reached 9 μmol·L^{-1} (Fmax = 568 nm) and the fluorescence intensity of the reaction solution reached the minimum value. The linear equation can be fitted by $Y = -114.969X + 675.182$ ($R^2 = 0.996$). The limit of detection (LOD) between NO and the reaction system is 0.15 μmol·L^{-1}, and the optical sensor shows high sensitivity to NO.

3.6 Selectivity

We studied the selectivity of the detection system for NO detection, including some of the normal interferences, such as NO_2^-, NO_3^-, K^+, Ca^{2+}, and glucose, recording the fluorescence intensity of reaction solution. As shown in Fig. 7, the fluorescence intensity of OPDox in the solution had no weakening when there were only 3 μmol·L^{-1} interferences in the reaction solution. When 3 μmol·L^{-1} of NO coexisted with 3 μmol·L^{-1} interferences in the reaction solution, the fluorescence intensity of OPDox in the solution weakened. The results showed no apparent interferences for NO detection, which confirmed that the optical sensor had relatively high selectivity.

3.7 Actual sample testing

Cell lysate was prepared for evaluating the NO detection capability of FMC detection strategy in actual samples. The fluorescence emission intensity of cell lysate samples at different concentrations of NO was collected to evaluate the NO recovery rate of the FMC detection strategy. Table 1 lists all the results. There was no NO in unmarked cell lysate. Then, we had the standard addition recovery experiment in the proper range for evaluating this method's detection potential for NO in the actual environment. We added 0.3, 1.0, 3.0, and 6.0 μmol·L^{-1} NO to the samples and repeated the experiment three times. As shown in Table 1, the interferences of positive samples (cell lysates) did not influence NO detection. The recovery rate was between 98.5% and 103.6%. The relative standard deviation was between 0.4% and 1.8%. The results showed that this sensing strategy has great application potential for actual samples in NO detection.

Conclusion

In this study, we detected NO in the atmosphere based on the catalytic performance of the metal-organic framework CuCo-PTC MOF. The metal-organic framework CuCo-PTC MOF material was synthesized by

the solvothermal method. NO was detected by the colour of the intermediates o-phenylenediamine and hydrogen peroxide. Finally, the realistic sample (NO in cell lysate) was used to evaluate the accuracy and practical application potential of the detection strategy. Compared with the previously reported NO detection methods, this detection strategy has the following advantages: (1) CuCo-PTC MOF was used as a catalyst of the sensing strategy, which sped up the reaction and lowered the temperature when the catalyst was not present. (2) Colourimetry is easy to operate and can get detection results more directly. (3) Fluorescence colourimetry methods have high sensitivity and selectivity. The actual sample (cell lysate) was collected by a fluorescence colourimetric sensing strategy. As the result shows, the sensing strategy has a high potential to detect NO in actual samples.

Declarations

Acknowledgments.

The authors greatly appreciate the financial support from the National Science Foundation of China (Grant Nos. 22074089, 22104078), the Chinese Postdoctoral Science Foundation (Grant No. 2020M672258), the Central Thousand Talents Plan (No. ZYQR201810151), the Key Scientific Research Projects of Colleges and Universities in Henan Province (No. 21A150043), and the East China Normal University for support.

Declaration of Competing Interest

The authors declare no competing financial interest.

References

1. Liu YM, Punckt C, Pope MA, Gelperin A, Aksay IA (2013) Electrochemical Sensing of Nitric Oxide with Functionalized Graphene Electrodes [J]. Acs Applied Materials & Interfaces, 5(23): 12624-12630. https://doi.org/1021/am403983g
2. Napoli C, Ignarro L, Chemistry (2001) Nitric oxide and atherosclerosis [J]. Nitric Oxide Biology & Chemistry 5(2):88–97. https://doi.org/10.1006/niox.2001.0337
3. Traub O, Bibber RV (1995) Role of nitric oxide in insulin-dependent diabetes mellitus-related vascular complications [J]. West J Med 162(5):439–445. https://doi.org/10.1620/tjem.176.61
4. Thejass P, Kuttan G (2007) Allyl isothiocyanate (AITC) and phenyl isothiocyanate (PITC) inhibit tumour-specific angiogenesis by downregulating nitric oxide (NO) and tumour necrosis factor-α (TNF-α) production [J]. Nitric Oxide 16(2):247–257. https://doi.org/10.1016/j.niox.2006.09.006
5. Harding AW, Brown SD, Thomas KM (1996) Release of NO from the combustion of coal chars [J]. Combust Flame 107(4):336–350. https://doi.org/10.1016/S0010-2180(96)00080-6

6. Crutzen PJ (1970) The influence of nitrogen oxides on the atmospheric ozone content [J]. Quarterly Journal of the Royal Meteorological 96(408):320–325. https://doi.org/10.1007/978-3-319-27460-7_3
7. Durham JL, Overton JH, Aneja VP (1967) Influence of gaseous nitric acid on sulfate production and acidity in rain [J]. Atmospheric Environment 1981, 15(6): 1059-1068. https://doi.org/10.1016/0004-6981(81)90106-2
8. Ridnour LA, Sim JE, Hayward MA, Wink DA, Martin SM, Buettner GR, Spitz DR (2000) A Spectrophotometric Method for the Direct Detection and Quantitation of Nitric Oxide, Nitrite, and Nitrate in Cell Culture Media [J]. Anal Biochem 281(2):223–229. https://doi.org/10.1006/abio.2000.4583
9. Adekunle AS, Lebogang S, Gwala PL, Tsele TP, Olasunkanmi LO, Esther FO, Boikanyo D, Mphuthi N, Oyekunle J, Ogunfowokan AO, Ebenso EE (2015) Electrochemical response of nitrite and nitric oxide on graphene oxide nanoparticles doped with Prussian blue (PB) and Fe2O3 nanoparticles [J]. RSC Adv 5:27759–27774. https://doi.org/10.1039/c5ra02008e
10. Goodwin JM, Chrestensen CA, Moomaw EW (2018) Detection of Nitric Oxide by Membrane Inlet Mass Spectrometry [J]. Nitric Oxide 1747:35–47. https://doi.org/10.1007/978-1-4939-7695-9_4
11. Jian P, Cheng W, Zhang H, Wang X, Tao Y, Duan L, a F CJ, M (2012) Luminescent Metal-Organic Frameworks for Selectively Sensing Nitric Oxide in an Aqueous Solution and in Living Cells [J]. Adv Funct Mater 22(8):1698–1703. https://doi.org/10.1002/adfm.201102157
12. Hetrick EM, Schoenfisch MH (2009) Analytical chemistry of nitric oxide [J]. Annual review of analytical chemistry (Palo Alto, Calif), 2: 409-433. https://doi.org/10.1146/annurev-anchem-060908-155146
13. Wu P, Jian W, Cheng H, Zhang X, Wang Y, Tao L, Duan C, J a F, M (2012) Luminescent Metal-Organic Frameworks for Selectively Sensing Nitric Oxide in an Aqueous Solution and in Living Cells [J]. Adv Funct Mater 22(8):1698–1703. https://doi.org/10.1002/adfm.201102157
14. Li Z, Li Y, Xing B et al (2018) OPD analysis and prediction in aero-optics based on dictionary learning[J]. Aerospace Systems 7(2):61–70. https://doi.org/10.1007/s42401-018-0020-1
15. Sun J, Wang B, Zhao X, Li ZJ, Yang XR (2016) Fluorescent and Colorimetric Dual-Readout Assay for Inorganic Pyrophosphatase with Cu^{2+}-Triggered Oxidation of *o*-Phenylenediamine [J]. Anal Chem 88(2):1355–1361. https://doi.org/10.1021/acs.analchem.5b03848
16. Nemiwal M, Gosu V, Zhang TC, Kumar D (2021) Metal organic frameworks as electrocatalysts: Hydrogen evolution reactions and overall water splitting [J]. Int J Hydrog Energy 46(17):10216–10238. https://doi.org/10.1016/j.ijhydene.2020.12.146
17. Bakhtiari N, Azizian S (2015) Adsorption of copper ion from aqueous solution by nanoporous MOF-5: A kinetic and equilibrium study [J]. J Mol Liq 206:114–118. https://doi.org/10.1016/j.molliq.2015.02.009
18. Tehrani MS, Zare-Dorabei R (2016) Competitive removal of hazardous dyes from aqueous solution by MIL-68(Al): Derivative spectrophotometric method and response surface methodology approach

[J]. Spectrochim Acta Part A Mol Biomol Spectrosc 160:8–18. https://doi.org/10.1016/j.saa.2016.02.002

19. Stock N, Biswas S (2012) Synthesis of Metal-Organic Frameworks (MOFs): Routes to Various MOF Topologies, Morphologies, and Composites [J]. Cheminform 43(16):933–969. https://doi.org/10.1002/chin.201216255
20. Li JR, Sculley J, Zhou HC (2012) Metal-Organic Frameworks for Separations [J]. Chem Rev 112(2):869–932. https://doi.org/10.1021/cr200190s
21. Kreno LE, Leong K, Farha OK, Allendorf M, Van Duyne RP, Hupp JT (2012) Metal-Organic Framework Materials as Chemical Sensors [J]. Chem Rev 112(2):1105–1125. https://doi.org/10.1021/cr200324t
22. Wang L, Han Y, Feng X, Zhou J, Qi P, Wang B (2016) Metal-organic frameworks for energy storage: Batteries and supercapacitors [J]. Coord Chem Rev 307:361–381. https://doi.org/10.1016/j.est.2018.12.025
23. Wang L, Zheng M, Xie Z (2018) Nanoscale metal-organic frameworks for drug delivery: a conventional platform with new promise [J]. Journal of Materials Chemistry B 6(5):707–717. https://doi.org/10.1039/c7tb02970e
24. Wang Q, Astruc D (2020) State of the Art and Prospects in Metal-Organic Framework (MOF)-Based and MOF-Derived Nanocatalysis [J]. Chem Rev 120(2):1438–1511. https://doi.org/10.1021/acs.chemrev.9b00223
25. Mccarver GA, Rajeshkumar T, Vogiatzis KD (2021) Computational catalysis for metal-organic frameworks: An overview [J]. Coord Chem Rev 436(18):213777. https://doi.org/10.1016/j.ccr.2021.213777
26. Li S, Zhai Y, Wei X, Zhang Z, Tang F (2021) Catalytic performance of MILB(V) and MIL1(V) MOFs for the selective catalytic reduction of NO with NH3 [J]. ChemCatChem 13(3):940–951. https://doi.org/10.1002/cctc.202001622

Tables

Table 1 Recovery study of the spiked determination of NO in cell lysates samples

Real Sample	Add NO （μM·L^{-1}）	Recycle NO （μM·L^{-1}）[a]	Recovery rate （%）	The relative standard deviation （n = 3）（%）
	0	Not detected	-	-
	0.300	0.295 ± 0.008	98.5	0.4
Cell lysates	1.000	1.021 ± 0.012	102.1	0.7
	3.000	3.081 ± 0.013	102.7	1.1
	6.000	6.216 ± 0.016	103.6	1.8

n is ± standard deviation (n = 3)

Figures

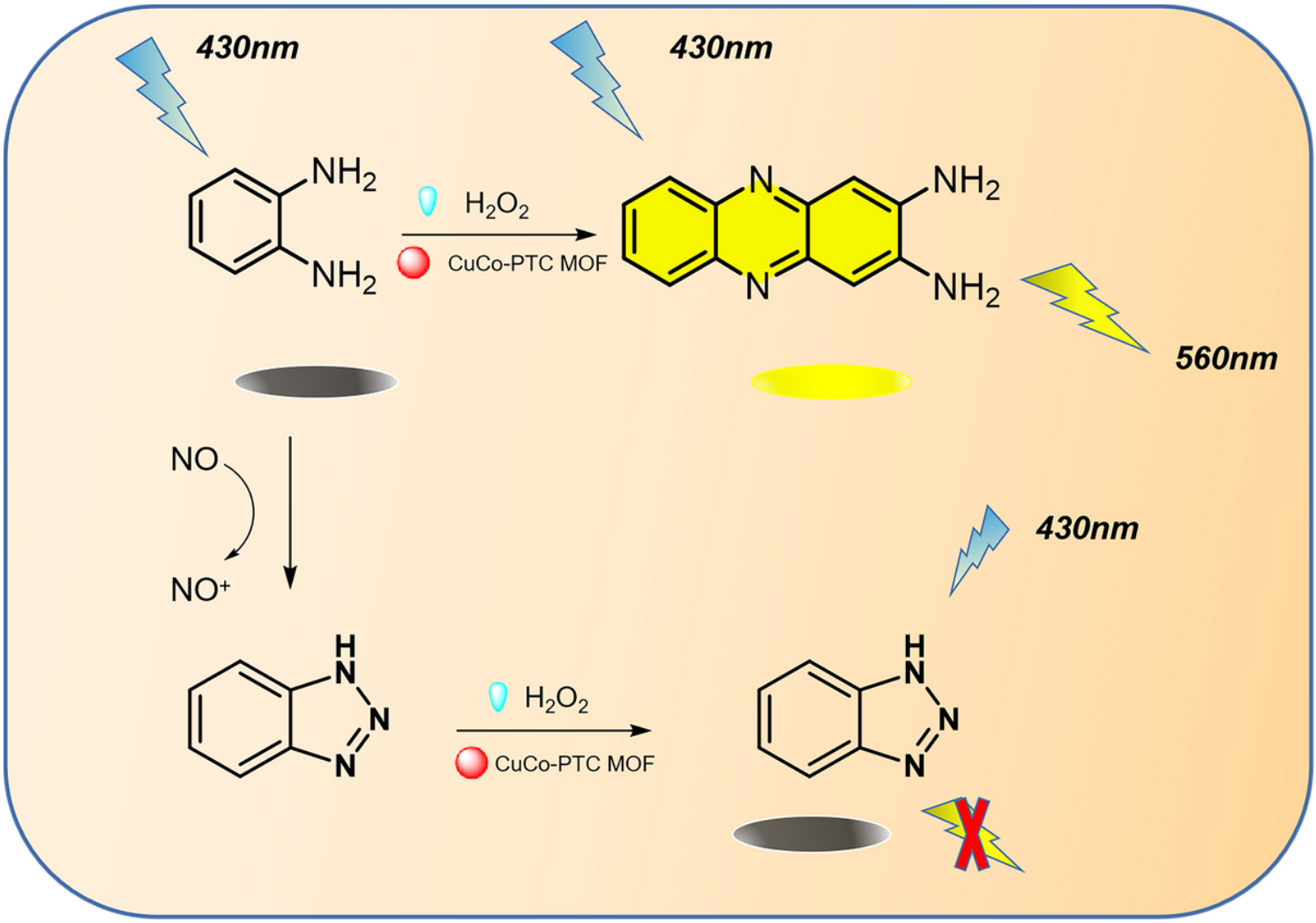

Figure 1

Schematic of fluorescence colourimetric detection of NO

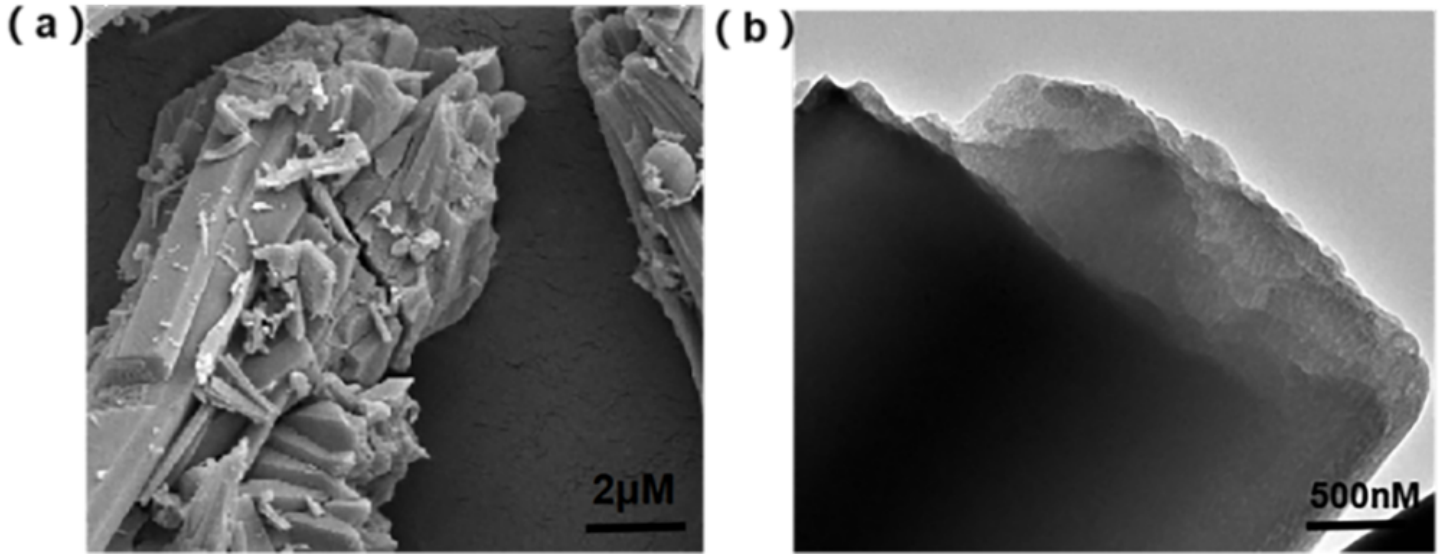

Figure 2

Microscopic images of CuCo-PTC MOF surface: **a** SEM image; **b** TEM image

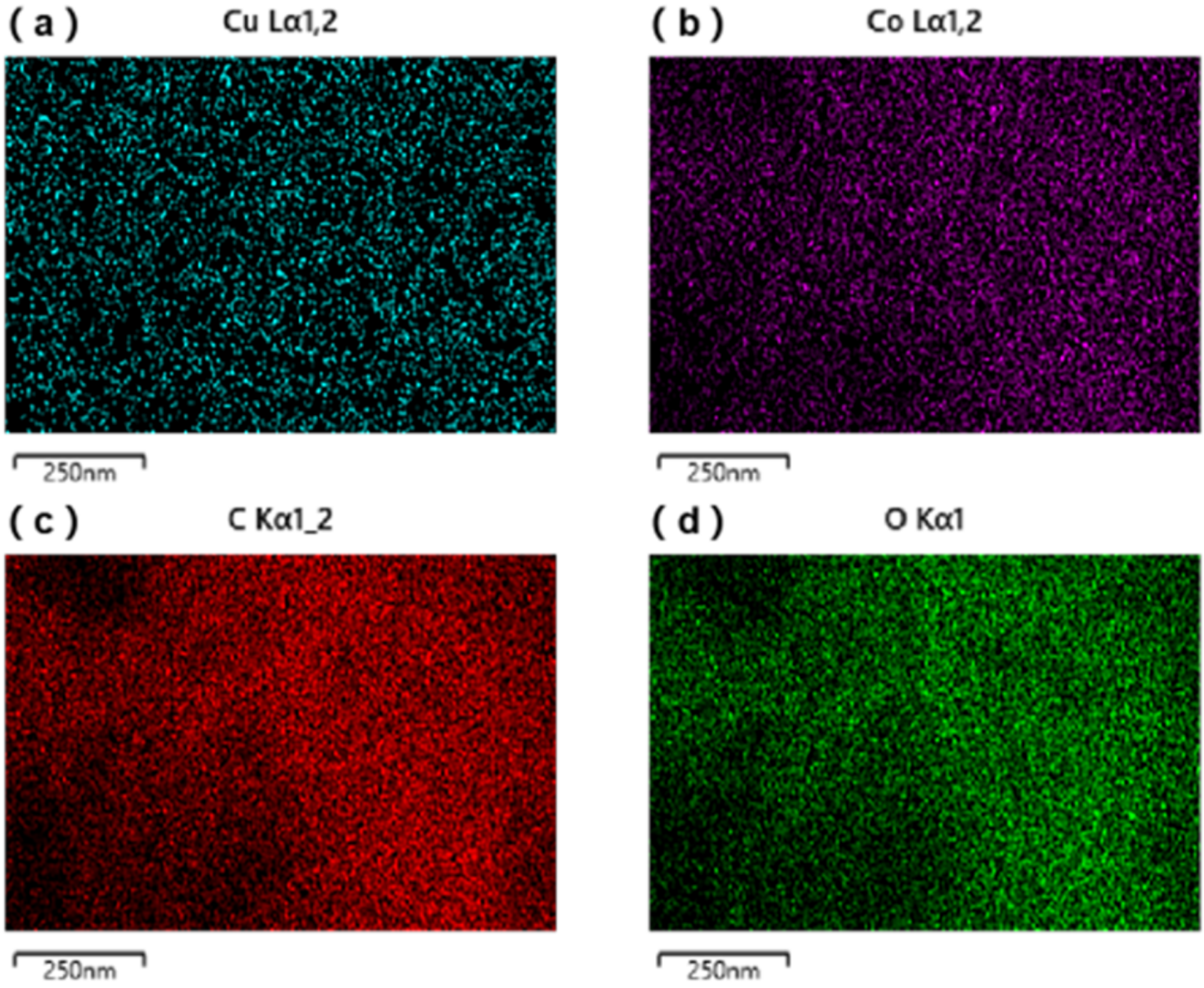

Figure 3

EDS elemental mapping of **a** Cu, **b** Co, **c** C, and **d** O in CuCo-PTC MOF

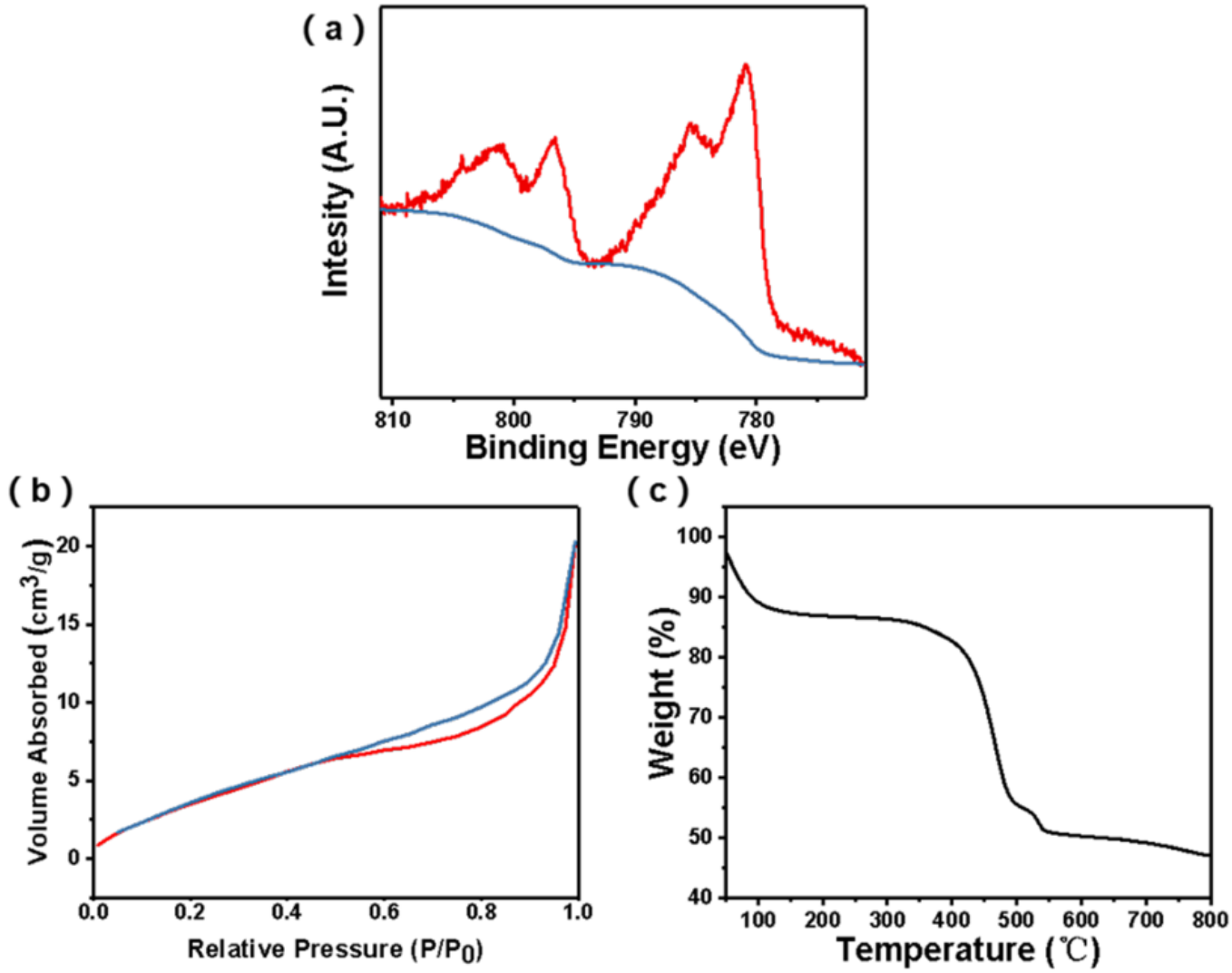

Figure 4

Investigation of the surface element composition and chemical state of CuCo-PTC MOF: **a** XPS spectra, **b** N_2 adsorption–desorption isotherms, **c** thermogravimetric curve

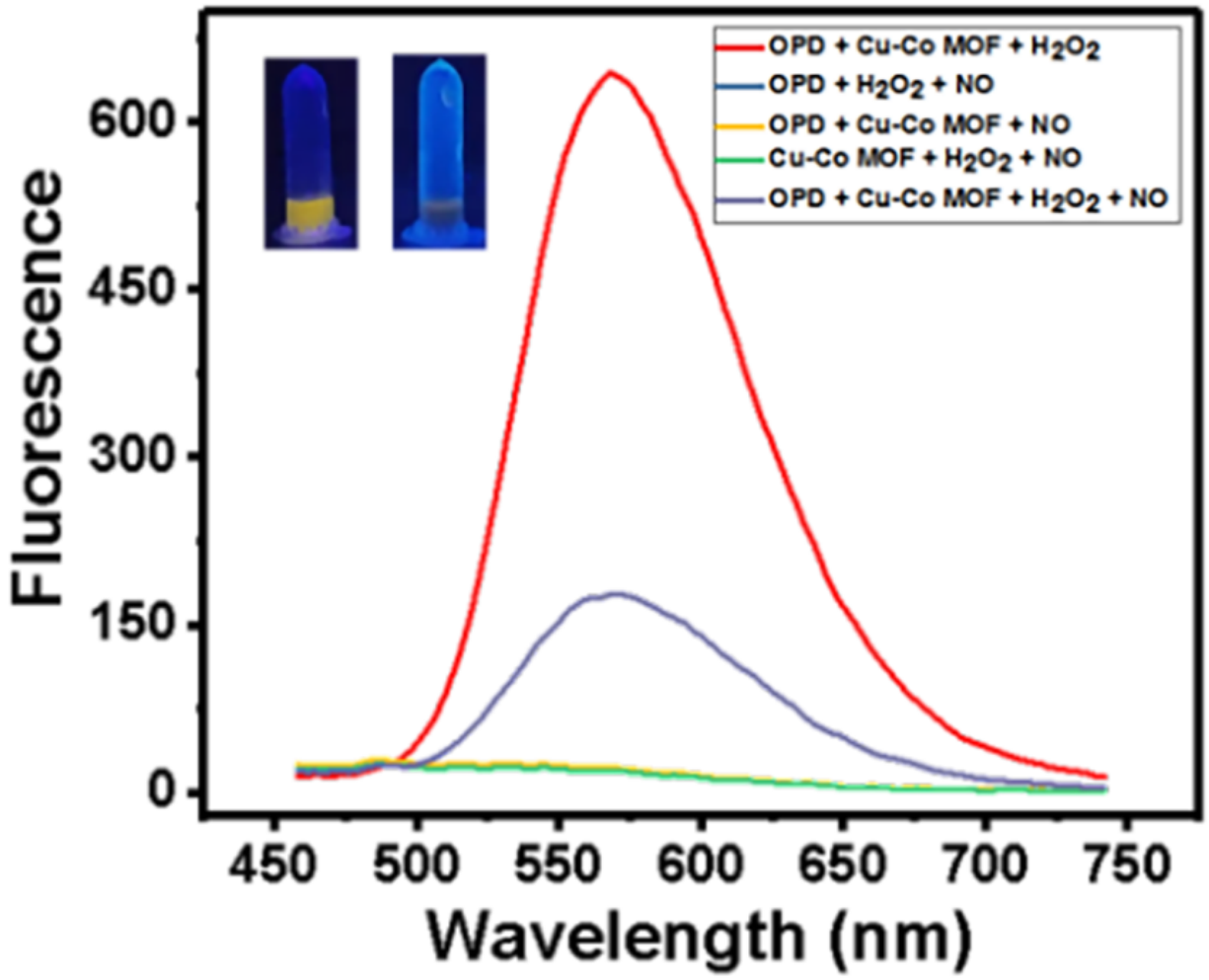

Figure 5

Changes in fluorescence intensity of reaction solution of 0.1 mol×L^{-1} PBS, 10 mg×L^{-1} CuCo-PTC MOF, 26 mmol×L^{-1} OPD, and 12 mol×L^{-1} hydrogen peroxide, before and after NO addition. The inset is the photo taken by a mobile phone under the 365 nm LED light before and after the reaction solution was added to NO under stable conditions

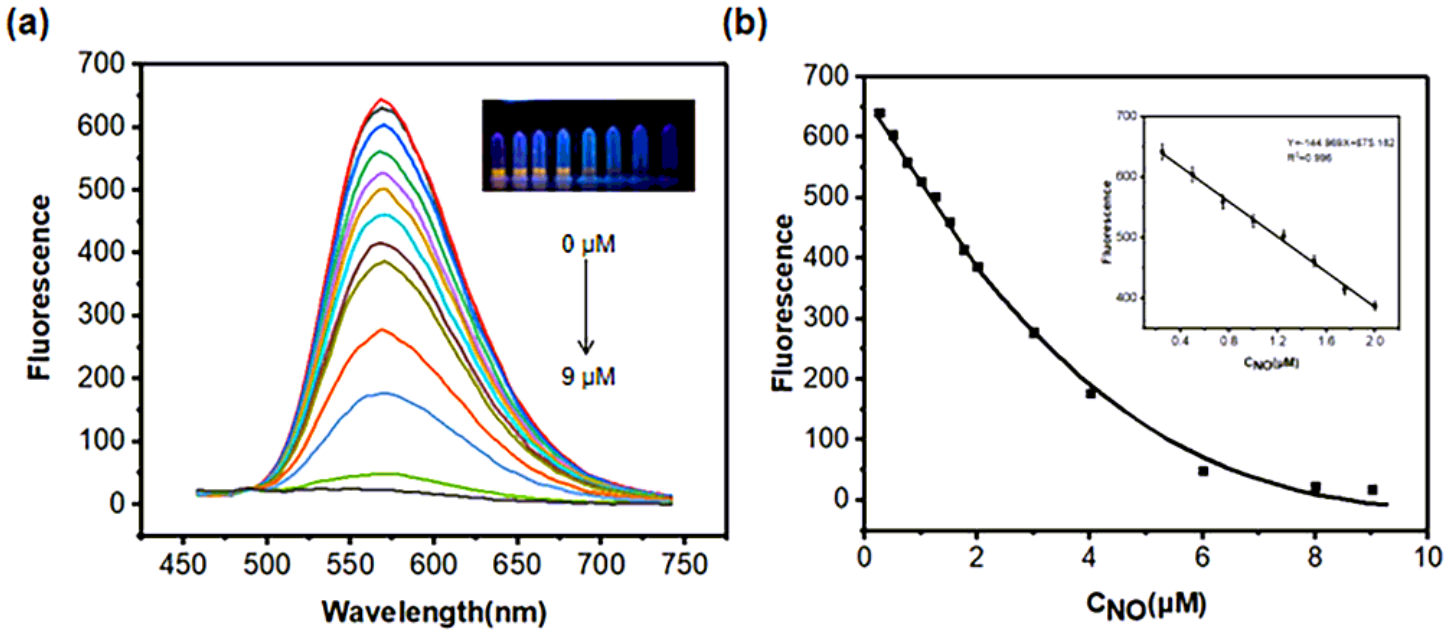

Figure 6

a In the solution of 0.1 mol×L^{-1} PBS, 8 mg×L^{-1} CuCo-PTC MOF, 24 mol×L^{-1} OPD and 16 mol×L^{-1} hydrogen peroxide, the fluorescence intensity of the reaction solution changes when the concentration of NO is in the range of 0–9 μmol×L^{-1}. The inset shows the solution colour change for different NO concentrations, photographed by mobile phone under an LED lamp with 365nm wavelength. **b** Relationship between the fluorescence intensity of reaction solution and the NO concentration at 520 nm

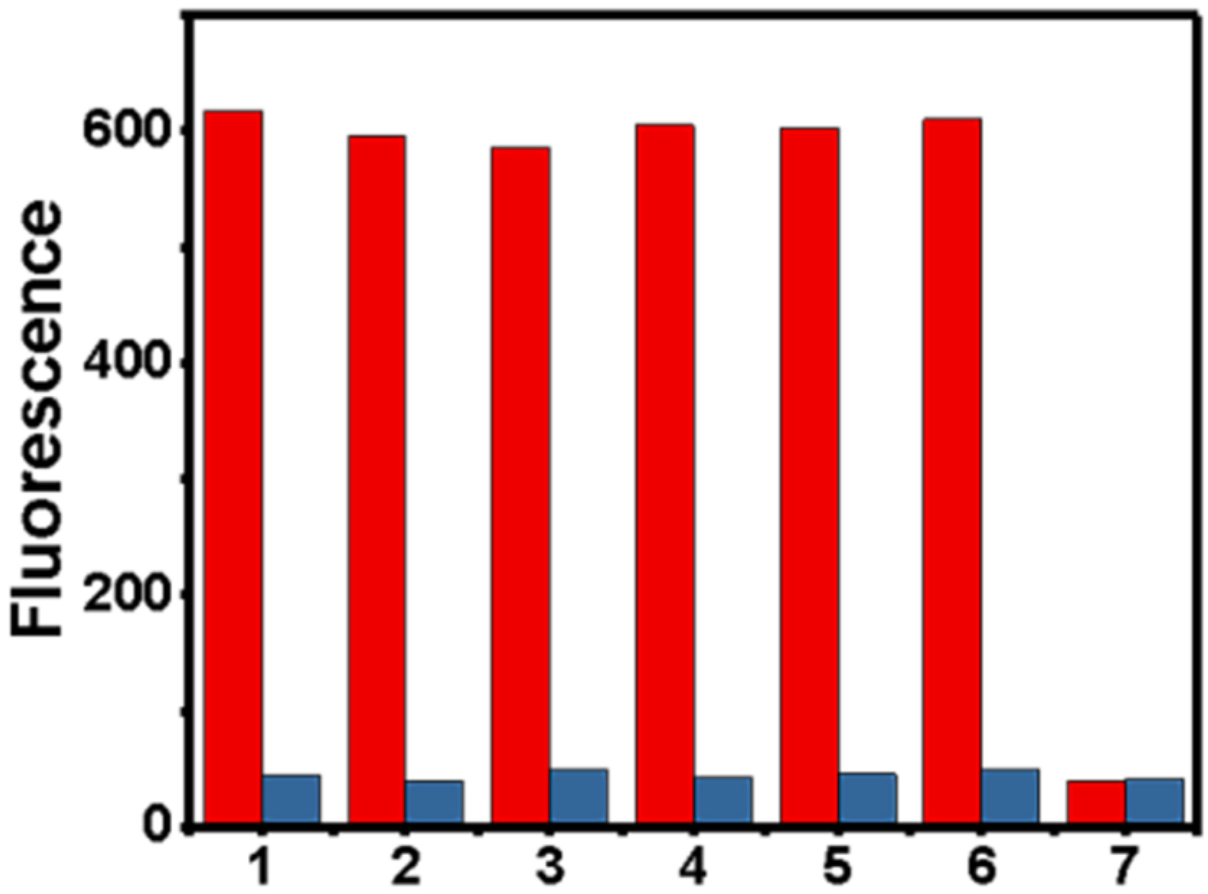

Figure 7

Change in maximum fluorescence intensity in response to the fluorescence colourimetric strategy of different species competing with NO (18 μmol·L^{-1}), 1–7: Blank, NO_3^-, NO_2^-, Ca^{2+}, Glucose, K^+, NO, respectively

Supplementary Files

This is a list of supplementary files associated with this preprint. Click to download.

- GraphicalAbstract.docx
- ElectronicSupplementaryMaterial.pdf